Available online at www.sciencedirect.com
ScienceDirect
Journal of Solid State Chemistry 180 (2007) 1325–1332
JOURNAL OF SOLID STATE CHEMISTRY
www.elsevier.com/locate/jssc

Dependence of nitrogen doping on TiO_2 precursor annealed under NH_3 flow

Xiaoming Fang*, Zhengguo Zhang, Qinglin Chen, Hongbing Ji, Xuenong Gao

The Key Laboratory of Enhanced Heat Transfer and Energy Conservation, Ministry of Education, School of Chemical and Energy Engineering, South China University of Technology, Guangzhou 510640, China

Received 27 November 2006; received in revised form 11 February 2007; accepted 12 February 2007
Available online 22 February 2007

Abstract

N-doped TiO_2 photocatalysts were prepared by annealing two different precursors, P25 and a TiO_2 xerogel powder under NH_3/Ar flow at 500, 550, and 600 °C. The xerogel powder prepared by peptizing $Ti(OH)_4$ with HNO_3 was composed of nanoparticles and had large specific surface area. During the annealing process, the xerogel powder underwent increase in crystallinity, grain growth and phase transformation, whereas P25 did not show obvious changes. Compared with the N-doped TiO_2 photocatalysts from P25, the N-doped TiO_2 photocatalysts from the xerogel powder possessed higher concentrations of the substitutional nitrogen and exhibited more obvious absorption in the visible light region. The N-doped TiO_2 photocatalysts from the xerogel powder exhibited obvious visible-light activities for photodegrading methylene blue and the sample prepared at 500 °C achieved the best performance with a rate constant (k) about 0.44 h^{-1}, whereas those from P25 did not exhibit improved visible-light activities.

Keywords: Photocatalysis; TiO_2; Visible-light active; Nitrogen doping

1. Introduction

Photocatalysis is one of the most interesting technologies in elimination of toxic organic compounds either in gas or in liquid phase [1]. TiO_2 is the most important inorganic photocatalyst due to its low cost, outstanding stability and highly efficient oxidative power [2,3]. However, the wide use of TiO_2 in photocatalysis is limited by its wide band gap (3.2 eV for anatase), which facilitates response to UV light. Therefore, numerous studies have been attempted to extend the photoresponse of TiO_2 further into the visible light region by coupling with organic dye sensitizers [4], by doping with transition metals [5], or by reducing with hydrogen [6]. Recently, since the report by Asahi et al. in 2001 [7], anionic non-metal (such as carbon, sulfur, fluorine, and nitrogen) doping has been recognized as a more appropriate approach [8–10]. Moreover, anion-doped TiO_2 photocatalysts are considered to be the second-generation photocatalytic materials [11], in which nitrogen-doped TiO_2 is the representative.

In the past 5 years, nitrogen-doped TiO_2 photocatalysts have been under extensive investigation, which mainly focus on the following aspects: the preparation, structure characterization and visible-light activity evaluation [12–16], the theoretical calculations of the electronic properties of N-doped TiO_2 to elucidate the origin of visible-light responses [17,18], and the investigation on the photocatalytic degradation process of some organic compounds over N-doped TiO_2 under visible light irradiation [19,20]. The methods for preparing nitrogen-doped TiO_2 powders are generally as follows: the hydrolysis of organic and inorganic titanium compounds with ammonia water followed by heating the resultant precipitates or their mixtures with urea [21,22], the nitridation of TiO_2 colloidal nanoparticles with alkylammonium salts at room temperature [23], the mechanochemical reaction of titania with hexamethylenetetramine or urea [24], the spray pyrolysis from a mixed aqueous solution containing $TiCl_4$ and an N-precursor [25], and the heat treatment of a TiO_2 precursor in an ammonia atmosphere [7,26,27]. Among the above

*Corresponding author. Fax: +86 20 8711 3870.
E-mail address: cexmfang@scut.edu.cn (X. Fang).

0022-4596/$ - see front matter © 2007 Elsevier Inc. All rights reserved.
doi:10.1016/j.jssc.2007.02.010

methods, the annealing of TiO_2 powder under NH_3 flow is the simplest and most applicable process. However, controversial ideas exist on the properties of the N-doped TiO_2 photocatalysts prepared by the process. On the one hand, Asahi et al. [7] and Irie et al. [26] reported that the N-doped TiO_2 photocatalysts prepared by treating the ST-01 anatase powders (Ishihara Sangyo Kaisha, Japan) in the NH_3 (67%)/Ar atmosphere, revealed optical absorption and photocatalytic activity under visible light irradiation and on the other hand, Mrowetz et al. [28] found that the N-doped TiO_2 catalyst prepared by treating a commercial anatase TiO_2 powder (Aldrich) under a NH_3 (80%)/Ar gas flow, failed to catalyze the oxidation of $HCOO^-$ into CO_2^- or of NH_3–OH^+ into NO_3^- under visible light illumination.

In the current work, two different TiO_2 powders were used as the precursors, and two series of N-doped TiO_2 photocatalysts were prepared by annealing the two precursors under NH_3/Ar flow at 500, 550, and 600 °C. The microstructures of the two series of N-doped TiO_2 photocatalysts were characterized by X-ray diffractometer (XRD) and X-ray photoemission spectroscopy (XPS), and were brought into comparison. The optical absorption and photocatalytic activities of the two series of N-doped TiO_2 photocatalysts in the visible light region were investigated, and intriguing results were obtained.

2. Experimental

2.1. Preparation of N-doped TiO_2 photocatalysts

The two TiO_2 precursors were the P25 TiO_2 powder (Nippon Aerosil Co., Ltd.) and a xerogel powder. The procedure for preparing the xerogel powder was as follows. $Ti(SO_4)_2$, ammonia, and HNO_3 were used as start materials, and were of analytical reagent grade. Firstly, 7% (wt%) of ammonia aqueous solution was added dropwise to $Ti(SO_4)_2$ aqueous solution to prepare $Ti(OH)_4$ precipitate. Then, after being filtrated and washed with distilled water five times, the precipitate was dispersed into an HNO_3 aqueous solution (HNO_3/TiO_2(mole) = 0.6) at 60 °C while stirring, and the precipitate was peptized and transformed to a transparent sol with pale blue tint. After being aged at 50 °C, the sol transformed to a gel. Finally, the xerogel powder was obtained by drying the TiO_2 gel at 50 °C followed by grinding, which was named FT. N-doped TiO_2 photocatalysts were prepared by annealing the two precursors under NH_3 (67%)/Ar flow at 500, 550, and 600 °C for 3 h. The N-doped TiO_2 products from P25 were called N-P25-500, N-P25-550, and N-P25-600, respectively. By analogy, the N-doped TiO_2 products from the FT xerogel powder were called N-FT-500, N-FT-550, and N-FT-600, respectively. As references, P25 and FT were annealed in the air at 550 °C for 3 h, and the products obtained were named O-P25-550 and O-FT-550.

2.2. Characterization

The TEM image of the xerogel powder was obtained using a transmission electron microscope (JEM-2010HR). The Brunnauer–Emmet–Teller (BET) surface areas of the precursors and their corresponding products were determined using nitrogen adsorption (Model ASAP 2010, Micromeritics, USA). XRD patterns of the precursors and their corresponding products were obtained using an X-ray diffractometer (Model X'pert PRO, PANalytical, Holand). The XPS data were obtained with an X-ray photoelectron spectrometer (Kratos AXis Ultra) using Al (monochromated) Kα radiation. The binding energies were referenced to the C1s line at 284.9 eV from adventitious carbon. Optical absorbance spectra of the precursors and their corresponding products were measured using the diffuse reflection method on a UV–vis spectrometer equipped with an integrating sphere setup (U-3010, Hitachi, Japan).

2.3. Photocatalytic activity evaluation

The photocatalytic activities of the samples were evaluated by measuring decomposition rates of methylene blue under visible light irradiation. The visible light was obtained by a 500 W Xenon lamp with a 420 nm cut-off filter, and its intensity was 100 mW/cm^2. Firstly, the powdered samples (about 200 mg) were dispersed into 200 mL 15 mg/L (C_i) of methylene blue aqueous solution stirring magnetically for 30 min to establish absorption/desorption equilibrium. Subsequently, 5 mL of the suspensions were sampled. After the suspensions were centrifuged at 2000 rpm, the concentrations (C_0) of the solutions were measured at 662 nm on a UV–vis spectrometer. Then, the Xenon lamp was switched on, and the aqueous suspensions containing methylene blue and powdered catalysts were irradiated under the Xenon lamp. At the given time intervals, 5 mL of the suspensions was taken from the suspensions and their concentrations were measured.

3. Results and discussion

3.1. Characterization of the TiO_2 xerogel powder

When the ammonia aqueous solution was added to the $Ti(SO_4)_2$ aqueous solution, an amorphous $Ti(OH)_4$ white precipitate was prepared. After the washed precipitate was dispersed into the HNO_3 aqueous solution stirring at 60 °C, the precipitate transformed to a transparent TiO_2 sol by peptization [29]. The TiO_2 xerogel was obtained by aging and drying the sol at 50 °C. The TEM image of the xerogel powder is shown in Fig. 1. It can be seen that the xerogel powder consisted of nanoparticles with good dispersibility, most of which were less than 10 nm in size. Furthermore, the BET specific surface area of the xerogel powder was measured to be as large as 236 m^2/g. It has been reported in our previous paper that the mesoporous nanocrystalline TiO_2 powders with a pore distribution centered at ca.

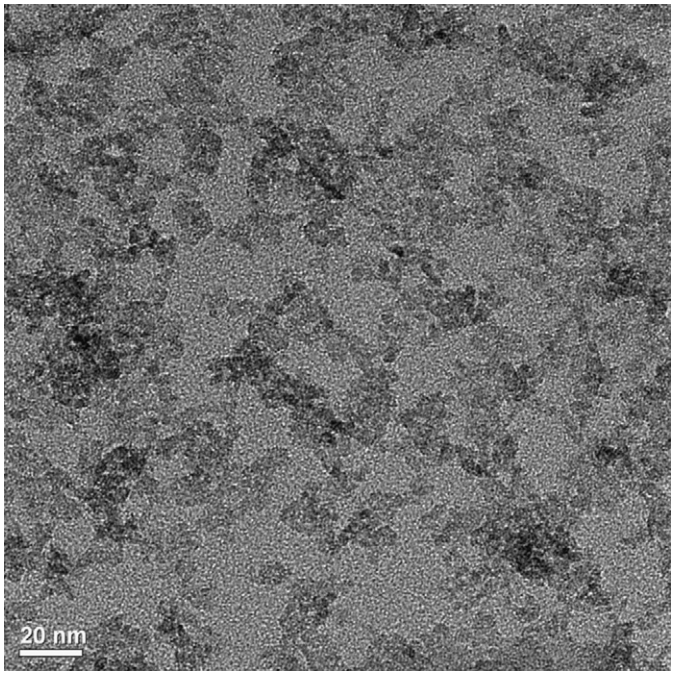

Fig. 1. TEM image of the FT xerogel powder.

40 nm were obtained by calcining the xerogel powders at 550 and 650 °C, and the mesopores disappeared after calcination at 750 °C [30]. It was revealed that, during the annealing process at the temperatures lower than 750 °C, the xerogel powder underwent the conglomeration of the nanoparticles to form mesoporous nanocrystalline TiO_2 powders.

3.2. Comparison on microstructures of N-doped TiO_2 powders from different precursors

3.2.1. XRD analysis

XRD patterns of the two precursors and their corresponding products are displayed in Fig. 2. The average grain sizes of anatase in the products were determined from the broadening of corresponding X-ray diffraction peaks by Scherrer's formula. The rutile fractions in the products were calculated based on the respective intensities of anatase and rutile peaks [31]. The values of the average grain sizes of anatase and rutile fractions in all the products are displayed in Table 1. It can be seen from Fig. 2(a) that the FT xerogel powder had anatase form with poor crystallinity. Since the temperatures for aging the sol and drying the gel were as low as 50 °C, it could be inferred that the anatase embryos were formed during the peptizing process at 60 °C with HNO_3 as the peptizer. It suggested that the amorphous $Ti(OH)_4$ precipitate conglomerations underwent directional arrangement to form the ordered structure of anatase during the peptization process. It can also be seen from Fig. 2(a) that, compared with FT, sharp diffractive peaks were observed for N-FT-500, N-FT-550, and N-FT-600, suggesting that the products with high

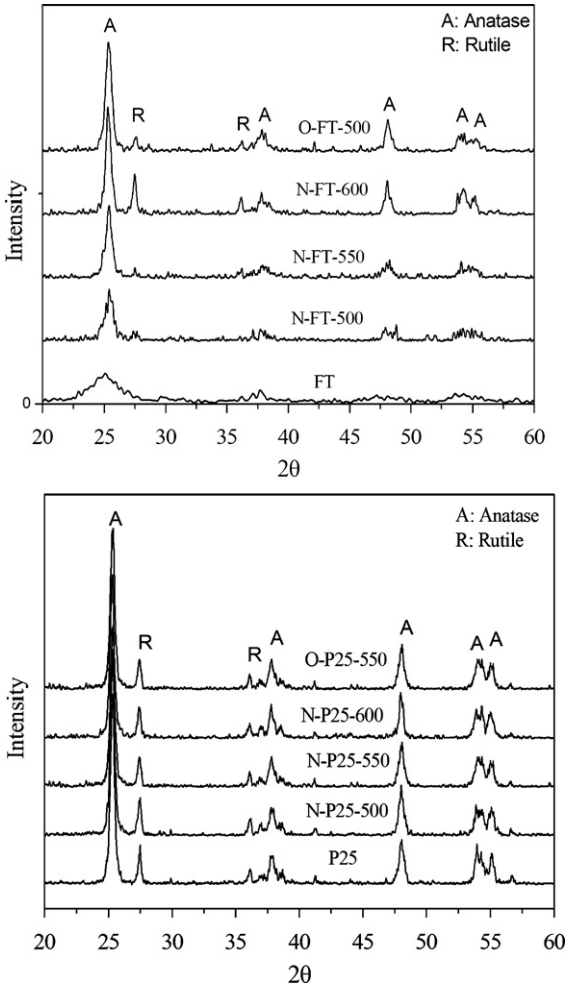

Fig. 2. XRD patterns of the two precursors and their corresponding products: (a) FT and (b) P25.

crystallinity were obtained accompanying the growth of the anatase grain, as shown in Table 1. The average grain sizes of anatase in N-FT-500, N-FT-550, and N-FT-600 were 10.4, 12.6, and 16.3 nm, respectively, indicating the average grain size of anatase in the N-doped TiO_2 powders from FT increased with the annealing temperature. The BET surface areas of N-FT-500, N-FT-550, and N-FT-600 were measured to be 70, 59, and 52 m^2/g, respectively. Compared with the precursor, the significant reduction in the BET specific surface areas of the products was due to the conglomeration of the TiO_2 nanoparticles during the annealing process to produce mesoporous nanocrystalline TiO_2 powders [30]. Furthermore, N-FT-500, N-FT-550, and N-FT-600 consisted of anatase in majority and rutile in minority, and their rutile fractions were 15%, 17%, and 39%, respectively. It was indicated that the rutile fraction in the N-doped TiO_2 powders from FT increased with the annealing temperature, especially at 600 °C. From the results it was revealed that, during the annealing process under NH_3/Ar flow, FT underwent the increase in crystallinity, grain growth, phase transformation from anatase to rutile and formation of mesoporous structure.

Table 1
Properties of the products from the two different precursors

Precursors	FT					P25		
Products	O-FT-550	N-FT-500	N-FT-550	N-FT-600	O-P25-550	N-P25-500	N-P25-550	N-P25-600
Color	White	Yellow	Yellow green	Dark green	White	Ivory	Light yellow	Dark gray
Average grain size of anatase	15.9	10.4	12.6	16.3	24.5	24.5	24.3	24.3
Phase composition								
Anatase (%)	80	85	83	61	75	74	75	73
Rutile (%)	20	15	17	39	25	26	25	27
BET specific surface area (cm^2/g)	53	70	59	52	60	65	62	58
N1s								
β-N (%)	0	10	44	70	0	6	39	53
γ-N_2 (%)	100	90	56	30	100	94	61	47
Substitutional N (at%)	0	0.081	0.28	0.81	0	0.012	0.035	0.63
Ti_{2P}								
Ti^{4+} (%)	96	91	83	55	100	100	97	23
Ti^{3+} (%)	4	9	17	45	0	0	3	77
Relative coefficient (R)	0.997	0.993	0.994	0.991	0.989	0.995	0.990	0.988
Rate constant (k) (h^{-1})	0.087	0.44	0.33	0.18	0.24	0.23	0.20	0.12

P25 is a commercial form of TiO_2 and is frequently used in photocatalytic studies [32]. The P25 TiO_2 powder that consists of anatase (75%) and rutile (25%) had ca. 25 nm in the average grain size of anatase, and its BET specific surface area was about 67 m^2/g. It can be seen from Fig. 2(b) and Table 1 that the intensities of the diffractive peaks for N-P25-500, N-P25-550, N-P25-600, and O-P25-550 were close to those of the diffractive peaks for P25, and the grain sizes of anatase and the rutile fractions in the products were almost the same. It suggested that P25 did not show obvious changes in the grain size of anatase and the rutile fraction during the annealing process at the temperature between 500 and 600 °C under NH_3 flow or in the air. Furthermore, the BET specific surface areas of N-P25-500, N-P25-550, N-P25-600, and O-P25-550 were measured to be 65, 62, 58, and 60 m^2/g, respectively, indicating that P25 also did not show significant change in the BET specific surface area after being annealed at the temperature between 500 and 600 °C.

From the above analyses, it was revealed that, different precursors underwent different changes during the annealing process under NH_3/Ar flow the temperature between 500 and 600 °C. Thus, the microstructure of the N-doped TiO_2 product was dependent not only on the annealing conditions but also on the property of the precursor used.

3.2.2. XPS analysis

Presently, XPS is generally used to characterize the substitution of the oxygen sites with nitrogen atoms in the titania structure. The global XPS profiles for the two series of products from different precursors are displayed in Fig. 3, and the insets in Fig. 3 show the corresponding N1s spectra. It can be seen from Fig. 3(a) that the N1s spectra for the N-doped TiO_2 powders from FT consisted of two peaks: one was centered at 396–397 eV and the other was centered at 400–401 eV; with the increase in the annealing temperature, the intensity of the peak at 396–397 eV obviously increased, whereas the intensity of the peak at 400–401 eV gradually decreased. The N1s XPS spectrum for O-FT-550 consisted of two peaks: one was centered at 400 eV and the other was centered at 402 eV. It can be seen from Fig. 3(b) that the N1s spectra for the N-doped TiO_2 powders from P25 also consisted of two peaks centered at 396–397 and 400–401 eV; the intensities of the former peaks for N-P25-500 and N-P25-550 were very low, whereas a significant increase in the intensity of the former peak was observed for N-P25-600. One peak centered at 400–401 eV was observed for O-P25-550.

In the reported papers concerning N-doped TiO_2, controversies exist on the assignment of the peak feature in N1s XPS for the N-doped TiO_2. Asahi et al. [7] reported that three peak structures at the binding energies of 402, 400, and 396 eV were observed for the $TiO_{2-x}N_x$ films and the peaks were assigned as atomic β-N (396 eV) and molecularly chemisorbed γ-N_2 (400 and 402 eV). Diawald et al. [33] assigned the N1s peak at 399.6 eV as the peak feature for the N-doped rutile single crystals and presented that the doping state of nitrogen is chemically bound to hydrogen and oxygen, and this form of nitrogen is most likely located in an interstitial site. In the N1s XPS spectrum of the N-doped TiO_2 nanomaterial with high N doping concentration (up to 8%), a broad binding energy peak centered at 401.3 eV was observed, which was attributed to O–Ti–N [34]; however, Gopinath [35] argued

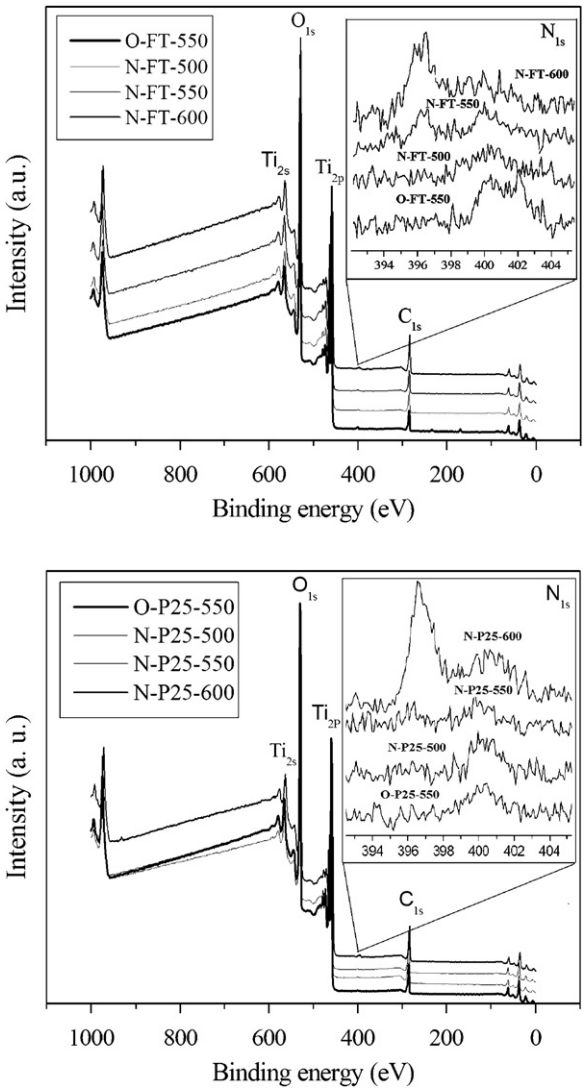

Fig. 3. N 1s XPS spectra for the corresponding products from the two precursors: (a) FT and (b) P25.

that the N1s peak at 398.2 eV should be attributed to the N state in O–Ti–N. Kisch and co-worker [36] prepared N-doped TiO_2 by calcining the hydrolysate of $TiCl_4$ with an ammonia aqueous solution. They found that no peak at 396–397 eV was observed in the N1s spectrum of the N-doped product, whereas a broad and weak peak at 404 eV was observed, which was attributed to the presence of hyponitrite. On the basis of the reports mentioned above, it could be presumed that the difference in the preparation methods may lead to the change in the N states in the N-doped TiO_2 products, thus to the distinction in the active sites responsible for their visible-light activities. It was obvious that the peak structures in the N1s XPS spectra for the N-doped TiO_2 powders from FT and P25 were similar to those reported by Asahi et al. [7]. According to their assignment, the percentages of the atomic β-N and chemisorbed γ-N_2 in the N-doped TiO_2 products were estimated by calculating the 396 eV peak areas and the 400 eV peak areas, and the values obtained are summarized in Table 1. Furthermore, the concentrations of the substitutional nitrogen were calculated by multiplying the percentages of the atomic β-N by the total nitrogen concentrations in all the N-doped TiO_2 products and are summarized in Table 1. It can be seen that the concentrations of the substitutional nitrogen in N-FT-500, N-FT-550, and N-FT-600 were 0.081, 0.28, and 0.81 at%, respectively, indicating that the concentrations of the substitutional nitrogen in the N-doped TiO_2 powders from FT increased with the annealing temperature, whereas only molecularly chemisorbed γ-N_2 existed in the product prepared in the air. Few substitutional nitrogen existed in the products prepared by annealing P25 under NH_3/Ar flow at temperatures 500 and 550 °C, and the remarkable increase in the concentration of the substitutional nitrogen occurred at the annealing temperature of 600 °C. Compared with the products from P25, the N-doped TiO_2 powders from FT at the same annealing temperatures possessed higher concentrations of the substitutional nitrogen. This result might be attributed to that, during the annealing process under NH_3/Ar flow, FT experienced the increase in crystallinity, grain growth, phase transformation from anatase to rutile and formation of mesoporous structure, whereas P25 did not.

Oxygen vacancy state in anatase TiO_2, which was generally correlative with the amount of Ti^{3+}, was below the lower end of the conduction band and acted as a recombination center for holes and electrons [26]. In order to investigate the oxygen vacancies existing in the N-doped TiO_2 products from the two precursors, the $Ti_2P_{3/2}$ peaks in all the products were fitted using the XPSPEAK software to separate the Ti^{4+} peaks and Ti^{3+} peaks. The percentages of Ti^{4+} and Ti^{3+} were estimated by comparing their peak areas, and the values obtained are summarized in Table 1. It can be seen that the Ti^{3+} percentages in N-FT-500, N-FT-550, and N-FT-600 were 9%, 17%, and 45%, respectively, indicating that the amount of Ti^{3+} in the N-doped TiO_2 products from FT increased with the annealing temperature, especially at 600 °C. It could be inferred that the amount of oxygen vacancy in the N-doped TiO_2 products from FT increased with the annealing temperature. The amount of Ti^{3+} in N-P25-500 and N-P25-550 was very low whereas the percentage of Ti^{3+} in N-P25-600 was as high as 77.26%, larger than that of Ti^{4+}. The high amount of Ti^{3+} in the products prepared at 600 °C resulted from the fact that the precursors were reduced by H_2, which was produced from the decomposition of NH_3 at over 550 °C [26]. It could be inferred that the amount of oxygen vacancy in N-P25-600 was very high, as compared with N-P25-500 and N-P25-550.

The above XPS analyses revealed that the concentration of substitutional nitrogen and the amount of oxygen vacancy in the N-doped TiO_2 powder were dependent not only on the annealing temperature but also on the precursor used.

3.3. Comparison on properties of N-doped TiO_2 powders from different precursors

3.3.1. Optical absorption in the visible light region

The colors of the two precursors and their corresponding products are also shown in Table 1. It was found that, after being annealed under NH_3/Ar atmosphere at different temperatures, the FT powder changed its color from white to yellow at 500 °C, to yellow green at 550 °C and to dark green at 600 °C, whereas O-FT-550 remained white. As for P25, O-P25-550 was as white as P25, N-P25-500 was ivory, N-P25-550 was light yellow, and N-P25-600 was dark gray. It indicated that P25 did not show obvious color change after being annealed at 500 and 550 °C, which revealed that the color of the N-doped TiO_2 powder was dependent on its precursor, and was distinct with the annealing temperature.

Fig. 4 shows the optical absorbance spectra obtained by diffuse reflection of the two precursors and their corresponding products. It could be seen in Fig. 4(a) that compared with FT, remarkable shifts of the absorption shoulders into the visible light region were observed for N-FT-500, N-FT-550, and N-FT-600, while little shift was observed for O-FT-550. It indicated that compared with O-FT-550 prepared by annealing FT in the air, the N-doped TiO_2 powders prepared from FT under NH_3/Ar flow were visible-light active. In more detail, the absorption edges of N-FT-500, N-FT-550, and N-FT-600 in the UV region (<400 nm) were almost the same as that of O-FT-550; in the range of wavelengths between 400 and 500 nm, significant absorption occurred for N-FT-500, N-FT-550, and N-FT-600, and their absorbance gradually increased with the annealing temperature; in the region of wavelengths longer than 500 nm, slight absorption was observed for N-FT-500, obvious absorption for N-FT-550, and remarkable absorption was observed for N-FT-600, indicating that the absorbance dramatically increased with the annealing temperature. It can be seen from Fig. 4(b) that, compared with P25, little shift of the absorption shoulder into the visible light region was observed for O-P25-550, slight shift for N-P25-500 and N-P25-550, and noticeable shift was observed for N-P25-600, especially at wavelengths longer than 500 nm. Furthermore, it was revealed that the N-doped TiO_2 powders prepared from the xerogel at the annealing temperature of 500 and 550 °C exhibited more obvious absorption in the visible light region, as compared with the N-doped TiO_2 powders prepared from P25 at the same annealing conditions; both significant absorptions were observed for N-FT-600 and N-P25-600, especially at wavelengths longer than 500 nm.

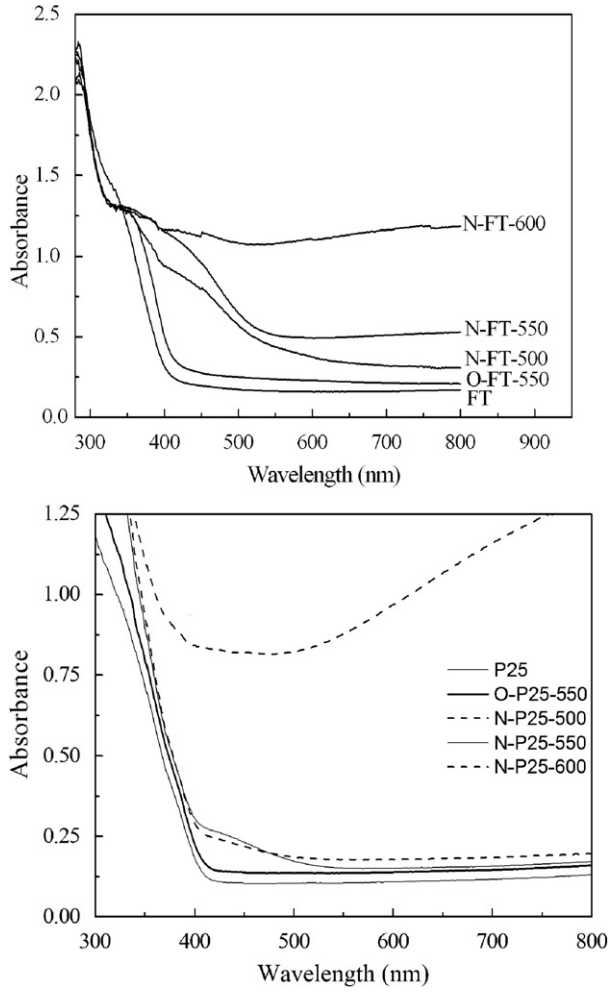

Fig. 4. Optical absorbance spectra obtained by diffuse reflection of the two precursors and their corresponding products: (a) FT and (b) P25.

More recently, several researchers focused their attention on the theoretical calculations of the electronic properties of N-doped TiO_2 to elucidate the origin of visible-light responses. Lin et al. [37] presented the results of spin-polarized density functional theory (DFT) calculations and optical absorption spectra that arise for a range of concentrations of substitutional nitrogen and oxygen vacancies in anatase TiO_2. Their research results showed that absorption below 500 nm was mainly due to nitrogen states located above the valence bands, whereas absorption above 500 nm was mainly caused by oxygen vacancies. Based on their research results and our XPS analyses, it could be concluded that the increase in the absorbances of the N-doped TiO_2 powders from FT in the range of wavelengths between 400 and 500 nm was attributed to the increase in the concentration of the substitutional nitrogen with the annealing temperature. The dramatic increase in the absorbances of the N-doped TiO_2 powders from FT at wavelengths greater than 500 nm was due to the remarkable increase in the amount of oxygen vacancy with the annealing temperature. The slight absorption for N-P25-500 and N-P25-550 in the visible light region was attributed to that few substitutional nitrogen existing in them. Noticeable absorption for N-P25-600 and N-FT-600 at wavelengths longer than 500 nm might be due to their high amount of oxygen vacancy.

3.3.2. Photocatalytic activities under visible light irradiation

The photocatalytic degrading curves for the methylene blue aqueous solution (15 mg/L) in the presence of the products from FT and P25 under visible light irradiation are displayed in Fig. 5. It was found that after the powdered samples have been dispersed into the methylene blue aqueous solution for 30 min under no light irradiation, a decrease in the concentration of methylene blue solution occurred, which was attributed to the sorption of the TiO_2-based powders for methylene blue molecules. The relative coefficients (R) and the slopes of the lines obtained by fitting linear $\ln(C_0/C)$ via irradiating time (t) are also shown in Table 1. It can be seen from Table 1 that the relative coefficients for all the products were close to 1, suggesting that the degradation of methylene blue in the presence of the photocatalysts was first-order kinetics reaction, and the slopes of the lines could be considered as the photodegradation reaction rate constants. It was obtained that the rate constants were 0.44 h^{-1} for N-FT-500, 0.33 h^{-1} for N-FT-550, 0.18 h^{-1} for N-FT-600, and 0.087 h^{-1} for O-FT-550, indicating that N-FT-500, N-FT-550, and N-FT-600 exhibited obvious visible-light activities for photodegrading methylene blue, whereas the visible-light activity of O-FT-550 was poor. It was revealed that annealing the FT xerogel powder under NH_3/Ar flow produced the visible-light-active photocatalysts. It could be inferred that the visible-light activities of N-FT-500, N-FT-550, and N-FT-600 might be attributed to that the remarkable shifts of the absorption shoulders for their optical absorbance spectra at wavelengths between 400 and 500 nm, which was due to the substitutional nitrogen existing in the products. The photocatalytic activities of the N-doped TiO_2 powders from FT gradually decreased with increase in annealing temperature, and N-FT-500 achieved the best performance. The decrease in the photocatalytic activities of the N-doped TiO_2 powders from FT with annealing temperature might be owing to the dramatical increase in the amount of oxygen vacancy with the annealing temperature, because the oxygen vacancies acted as recombination centers for holes and electrons [26].

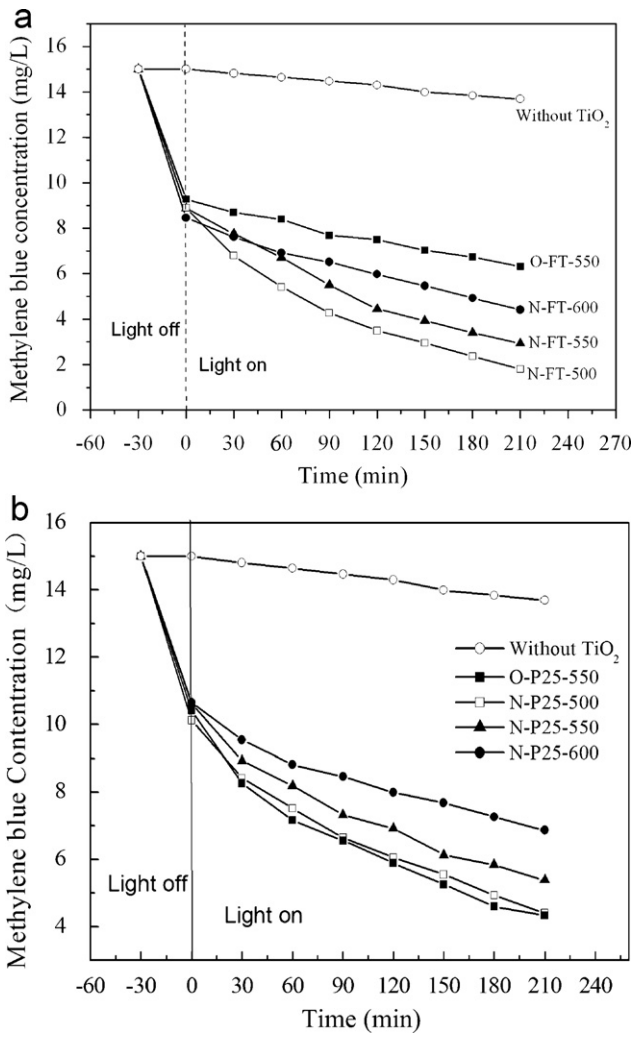

Fig. 5. Photocatalytic degradation curves of methylene blue under visible light irradiation in presence of the products from the two precursors: (a) FT and (b) P25.

As for the N-doped TiO_2 powders from P25, intriguing results were obtained. The rate constants were 0.24 h^{-1} for O-P25-550, 0.23 h^{-1} for N-P25-500, 0.20 h^{-1} for N-P25-550, and 0.12 h^{-1} for N-P25-550, respectively, indicating that the photocatalytic activities of N-P25-500 and N-P25-550 were comparable to that of O-P25-550, and N-P25-600 exhibited the worst photocatalytic activity. It was revealed that annealing P25 under NH_3/Ar flow did not produce the photocatalysts with improved visible-light activity, as compared with the product prepared in the air. Recently, there are several papers reporting that P25 exhibited photocatalytic activity under visible light irradiation [38,39]. It had been revealed from the above XRD analyses that P25 did not show obvious changes in the grain size and rutile fraction during the annealing process at the temperature between 500 and 600 °C under NH_3 flow or in the air. It was reasonable that O-P25-550 was also visible-light active. Since only slight shifts of the absorption shoulders into the visible light region at wavelength between 400 and 500 nm were observed for N-P25-500 and N-P25-550, and few oxygen vacancies existed in them, it could be inferred that the visible-light activities of N-P25-500 and N-P25-550 were comparable to these of O-P25-550. The worst visible-light activity for N-P25-600 was owing to its large amount of oxygen vacancy.

It was found that compared with the N-doped TiO_2 powders from P25, the N-doped TiO_2 powders from FT exhibited excellent photocatalytic activities under visible light irradiation, especially at the annealing temperature of 500 and 550 °C. The photocatalytic activity of the N-doped TiO_2 powder was relative to its specific surface area, grain size, phase composition, substitutional nitrogen concentration and oxygen vacancy amount. Based on the above XRD and XPS analyses, it was inferred that compared with N-P25-500 and N-P25-550, N-FT-500 and N-FT-550 possessed comparative specific surface area, smaller grain size, less rutile fraction, higher concentration of the

substitutional nitrogen and comparative amount of oxygen vacancy, which probably resulted in their more excellent photocatalytic activities. It was concluded from the above results that when N-doped TiO_2 was prepared by annealing a TiO_2 precursor under NH_3 flow, the visible-light activity of the N-doped TiO_2 photocatalyst was not only dependent on the annealing conditions but also relative to the precursor used. It is important to select a suitable precursor for preparing the N-doped TiO_2 photocatalysts with high visible-light activity.

4. Conclusions

The xerogel was composed of nanoparticles and had large specific surface area. During the annealing process at the temperature between 500 and 600 °C, FT experienced the increase in crystallinity, grain growth and phase transformation from anatase to rutile, whereas P25 did not show obvious change in the grain size and rutile fraction. Compared with the products from P25, the N-doped TiO_2 powders from FT at the same annealing temperatures possessed higher concentrations of the substitutional nitrogen and exhibited more obvious absorption in the visible-light region. Compared with the product prepared by annealing the xerogel in the air, the N-doped TiO_2 powders prepared from the xerogel under NH_3/Ar flow exhibited obvious visible-light activities for photodegrading methylene blue, and the sample prepared at 500 °C achieved the best performance with a rate constant (k) about $0.44\,h^{-1}$. It was found that annealing P25 under NH_3/Ar flow did not produce the photocatalysts with improved visible-light activity. It is important to select a suitable precursor for preparing the N-doped TiO_2 photocatalysts with high visible-light activity.

Acknowledgments

This work was supported by the National Natural Science Foundation of China (Project no. 20573038) and the project (2004CCA03100) from Ministry of Science and Technology of the People's Republic of China.

References

[1] M. Hoffman, S. Martin, W. Choi, Chem. Rev. 95 (1995) 69.
[2] A. Fujishima, T.N. Rao, D.A. Tryk, J. Photochem. Photobiol. C 1 (2000) 1.
[3] S.A. Bilmes, P. Mandelbaum, F. Alvarez, N.M. Victoria, J. Phys. Chem. B 104 (2000) 9851.
[4] T. Samuel, C. Cheury, Chemosphere 36 (1998) 2461.
[5] D. Dvoranová, V. Brezová, M. Mazúr, M.A. Malati, Appl. Catal. B: Environ. 37 (2002) 91.
[6] I. Nakamura, N. Negishi, S. Kutsuna, T. Ihara, S. Sugihara, K. Takeuchi, J. Mol. Catal. A: Chem. 161 (2000) 205.
[7] R. Asahi, T. Morikawa, T. Ohwaki, K. Aoki, Y. Taga, Science 293 (2001) 269.
[8] J.C. Yu, M. Zhou, B. Cheng, X. Zhao, J. Mol. Catal. A: Chem. 246 (2006) 176.
[9] J.C. Yu, J.G. Yu, W.K. Ho, Z.T. Jiang, L.Z. Zhang, Chem. Mater. 14 (2002) 3808.
[10] N. Venkatachalam, A. Vinu, S. Anandan, B. Arabindoo, V. Murugesan, J. Nanosci. Nanotechnol. 6 (2006) 2499.
[11] H. Wang, J.P. Lewis, J. Phys. Condens. Matter 18 (2006) 421.
[12] T. Lindgren, J.M. Mwabora, E. Avendano, J. Jonsson, A. Hoel, C.G. Granqvist, S.E. Lindquist, J. Phys. Chem. B 107 (2003) 5709.
[13] O. Diwald, T.L. Thompson, T. Zubkov, E.G. Goralski, S.D. Walck, J.T. Yates Jr., J. Phys. Chem. B 108 (2004) 6004.
[14] S. Livraghi, A. Votta, M.C. Paganini, E. Giamello, Chem. Commun. 4 (2005) 498.
[15] S. Sato, R. Nakamura, S. Abe, Appl. Catal. A 284 (2005) 131.
[16] A. Oriov, M.S. Tikhov, R.M. Lambert, Co. R. Chim. 9 (2006) 794.
[17] Y. Wang, D.J. Doren, Solid State Commun. 136 (2005) 186.
[18] J.Y. Lee, J. Park, J.H. Cho, Appl. Phys. Lett. 87 (2005) (Art No. 011904).
[19] Y. Irokawa, T. Morikawa, K. Aoki, S. Kosaka, T. Ohwaka, Y. Taga, Phys. Chem. Chem. Phys. 8 (2006) 1116.
[20] T. Tachikawa, Y. Takai, S. Yojo, M. Fujitsuka, H. Irie, K. Hashimoto, T. Majima, J. Phys. Chem. B 110 (2006) 13158.
[21] T. Ihara, M. Miyoshi, Y. Iriyama, O. Matsumoto, S. Sugihara, Appl. Catal. B: Environ. 42 (2003) 403.
[22] K. Kobayakawa, Y. Murakami, Y. Sato, J. Photochem. Photobiol. A: Chem. 170 (2005) 177.
[23] C. Burda, Y.B. Lou, X.B. Chen, A.C.S. Samia, J. Stout, J.L. Gole, Nano Lett. 3 (2003) 1049.
[24] S. Yin, K. Ihara, M. Komatsu, Q.W. Zhang, F. Saito, T. Kyotani, T. Sato, Solid State Commun. 137 (2006) 132.
[25] D. Li, H. Haneda, S. Hishita, N. Ohashi, Mater. Sci. Eng. B 117 (2005) 67.
[26] H. Irie, Y. Watanabe, K. Hashimoto, J. Phys. Chem. B 107 (2003) 5483.
[27] B. Kosowska, S. Mozia, A.W. Morwski, B. Grzmil, M. Janus, K. Kalucki, Sol. Energy Mater. Sol. Cell 88 (2005) 269.
[28] M. Mrowetz, W. Balcerski, A.J. Colussi, M.R. Hoffmann, J. Phys. Chem. B 108 (2004) 17269.
[29] N. Yao, G.X. Xiong, Y.H. Zhang, W.S. Yang, Sci. China B 31 (2001) 355.
[30] X.M. Fang, Z.G. Zheng, Q.L. Chen, Rare Metal Mater. Eng., in press.
[31] R.A. Spurr, W. Mayers, Anal. Chem. 29 (1957) 760.
[32] R.I. Bickley, T. Gonzalez-Carreno, J.S. Lees, L. Palmisano, R.J.D. Tilley, J. Solid State Chem. 92 (1991) 178.
[33] O. Diawald, T.L. Tompson, T. Zubkov, E.G. Goralski, S.D. Walck, J.T. Yates, J. Phys. Chem. B 108 (2004) 6004.
[34] X.B. Chen, C. Burda, J. Phys. Chem. B 108 (2004) 15446.
[35] C.S. Gopinath, J. Phys. Chem. B 110 (2006) 7079.
[36] S. Sakthivel, H. Kisch, Chemphyschem 4 (2003) 487.
[37] Z.S. Lin, A. Orlov, R.M. Lambert, M.C. Payne, J. Phys. Chem. B 109 (2005) 20948.
[38] S.W. Yang, L. Gao, J. Am. Ceram. Soc. 87 (2004) 1803.
[39] R. Silveyra, L.D.T. Saenz, W.A. Flores, V.C. Martinez, A.A. Elguezabal, Catal. Today 107/108 (2005) 602.